frontiers in Forests and Global Change

TYPE Original Research
PUBLISHED 27 July 2026
DOI 10.3389/ffgc.2026.1914270

OPEN ACCESS

EDITED BY
Manuel Jesús Cach Pérez,
El Colegio de la Frontera Sur, Mexico

REVIEWED BY
Mohammad Javad Ahmadi-Lahijani,
Ferdowsi University of Mashhad, Iran
Mirna Valdez-Hernández,
Unidad Chetumal, Mexico

*CORRESPONDENCE
Shucai Zeng
✉ sczeng@scau.edu.cn
Shuangshuang Chu
✉ chushsh@jxau.edu.cn

RECEIVED 20 June 2026
REVISED 06 July 2026
ACCEPTED 10 July 2026
PUBLISHED 27 July 2026

CITATION
Quan H, Lu J, Zeng S and Chu S (2026) Balancing growth, resource efficiency and soil greenhouse gas emissions: optimal water-fertilizer coupling for *Chukrasia tabularis* seedlings.
Front. For. Glob. Change 9:1914270.
doi: 10.3389/ffgc.2026.1914270

Balancing growth, resource efficiency and soil greenhouse gas emissions: optimal water-fertilizer coupling for *Chukrasia tabularis* seedlings

Hongting Quan[1], Jie Lu[1], Shucai Zeng[1]* and Shuangshuang Chu[2]*

[1]College of Forestry and Landscape Architecture, South China Agricultural University, Guangzhou, Guangdong, China, [2]College of Forestry, Jiangxi Agricultural University, Nanchang, China

Excessive and unregulated management of water and fertilizer limits the productivity of *Chukrasia tabularis* (*C. tabularis*) plantations in subtropical regions. A two-factor factorial potted experiment was conducted using one-year-old *C. tabularis* seedlings. Three soil water content levels (95%, 75%, and 55% field capacity) and four compound fertilizer rates (0, 6, 12, and 18 g pot^{-1}) were established, with the treatment of 75% field capacity and 0 g pot^{-1} fertilizer serving as the control (CK). Soil water content emerged as the dominant factor controlling *C. tabularis* seedling growth; furthermore, water and fertilizer exhibited a highly significant interaction effect on total biomass and root dry weight ($p < 0.001$). At the 12 g pot^{-1} fertilizer rate, seedlings grown at 55% field capacity produced 35% more total biomass than those at 75% field capacity, and 224% more than CK. It also raised root dry weight by 32% over the control. But 95% field capacity reduced growth under all fertilizer treatments. Under the 55% field capacity condition, nitrogen and potassium accumulation at the 12 g pot^{-1} fertilizer rate increased by 701% and 318%, respectively, compared to CK. In contrast, the 95% field capacity condition caused severe root hypoxia and nutrient leaching, effectively negating the benefits of fertilization and leading to negative apparent fertilizer use efficiency for phosphorus and potassium. At 55% field capacity, the observed CH_4 patterns suggested a potential shift from net emission to net uptake under selected treatments. A combined PCA-EWM-TOPSIS model demonstrated that a field capacity of 55% combined with 12 g pot^{-1} compound fertilizer achieved an optimal balance among growth benefits, resource use efficiency, and ecological trade-offs.

KEYWORDS
***Chukrasia tabularis*, comprehensive evaluation, plant growth, water and fertilizer coupling, water use efficiency**

1 Introduction

Mineral nutrients are essential for tree growth and metabolic processes, and fertilization is often necessary in nutrient-poor environments (Binkley and Fisher, 2019). However, excessive fertilization can disrupt the source-sink relationships in plants and lead to severe environmental issues, including soil leaching and increased greenhouse gas emissions (Wright et al., 2011; Rabbai et al., 2024). Importantly, the availability of soil water can significantly influence the outcomes of fertilization, resulting in divergent growth and environmental effects under varying soil water contents. While studies have shown that a combined supply of water and nutrients can greatly enhance stand productivity (Campoe et al., 2013), research frequently overlooks the potential negative effects of mismatched water and fertilizer combinations on tree seedlings. Without a clear understanding of how different soil water levels interact with specific fertilizer rates to influence seedling growth and resource utilization, forest managers risk either wasting resources or damaging young plants through inappropriate management practices.

Soil water and mineral nutrients are critical environmental factors that govern tree growth, photosynthesis, and resource use efficiency. These two factors are closely interconnected within the soil–plant system, with their interaction defining the growth potential of trees (Chen et al., 2023; Luo et al., 2024). While previous studies have demonstrated that water availability improves fertilizer use efficiency and that proper fertilization enhances tree tolerance to water stress (Campoe et al., 2013; Tariq et al., 2017), most existing research has focused on agronomic crops or common fruit trees, such as olives (Alderotti et al., 2025). High-value timber species, such as *Chukrasia tabularis* (*C. tabularis*), possess unique physiological traits and growth requirements. Consequently, findings from other species cannot be directly applied to guide the silviculture of *C. tabularis*, and its specific response to the coupling of water and fertilizer remains poorly understood.

Chukrasia tabularis, commonly known as Chickrassy or Chittagong wood, is a high-value, fast-growing broadleaved tree of the family Meliaceae, valued for its reddish-brown heartwood in furniture manufacturing, veneer production, and construction timber, and increasingly planted for urban greening and ecological restoration in subtropical China. As a species native to well-drained upland forests across tropical and subtropical regions (Islam et al., 2018), it is known to be sensitive to excessive soil moisture and poorly aerated substrates, which motivates the water-fertilizer coupling design of this study. Soils in South China typically exhibit poor water retention capacity and low nutrient availability, severely limiting tree productivity (Wilson et al., 2004). Furthermore, current management practices often rely on excessive watering and fertilization without coordinating these inputs. This approach not only wastes resources and reduces efficiency but also leads to soil nutrient leaching (An et al., 2022; Hussain et al., 2025). Despite these practical issues, few studies have quantified the interactive effects of soil water content and fertilizer rates on *C. tabularis* seedlings. Without precise data on the coupling of water and fertilizer, it is challenging to develop scientifically sound management practices aimed at maximizing seedling growth and resource efficiency.

We conducted a two-factor factorial potted experiment using one-year-old *C. tabularis* seedlings. The treatments included three levels of soil water contents (95%, 75%, and 55% of field capacity) and four rates of compound fertilizer (0, 6, 12, and 18 g pot^{-1}). We measured seedling growth, nutrient uptake, photosynthesis, water use efficiency, apparent fertilizer use efficiency, and soil greenhouse gas emissions. The objectives of this study were to: (1) quantify the effects of combined soil water and fertilizer levels on seedling growth, resource use efficiency, and soil greenhouse gas emissions of *C. tabularis* seedlings; and (2) identify the optimal water and fertilizer management regime using a multi-index evaluation model that integrates principal component analysis (PCA), the entropy weight method (EWM), and the Technique for Order of Preference by Similarity to Ideal Solution (TOPSIS). This study provides valuable insights to enhance seedling productivity and nutrient-use efficiency while mitigating soil greenhouse gas emissions, thereby offering significant support for the sustainable cultivation and ecological application of this species.

2 Materials and methods

2.1 Study site

The experiment was conducted in a greenhouse at South China Agricultural University, Guangzhou, China (113°21.8′-113°22.3′E, 23°09.5′-23°09.9′N). The site falls within the south subtropical monsoon climate zone. During the experimental period, air temperature fluctuated between 5.5 °C and 35.0 °C, with a mean air temperature of 22.8 °C. Temperature data were recorded by an automatic weather recorder (Figure 1).

2.2 Plant and soil parameters

One-year-old *C. tabularis* seedlings were purchased from Guangzhou Deyuan Forestry Co., Ltd. We selected healthy seedlings with uniform growth, featuring an initial mean height of 33.33 cm and a ground diameter of 2.74 mm. A commercial forestry-specific

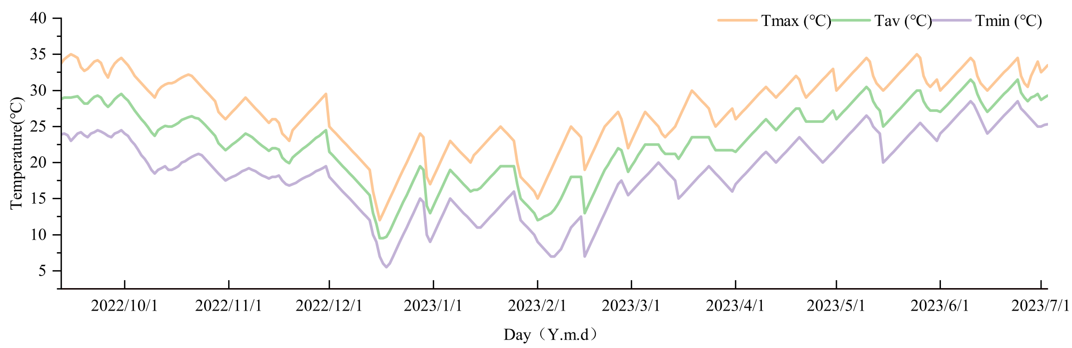

FIGURE 1
Temperature data during the experiment. T_{av} (°C) is the daily average temperature, T_{max} (°C) is the daily maximum temperature, T_{min} (°C) is the daily minimum temperature.

TABLE 1 Basic physicochemical properties of the experimental soil.

Indicator	Value
pH	6.70 ± 0.00
Electrical conductivity (μs·cm^{-1})	120.4 ± 4.10
Soil organic matter (g·kg^{-1})	3.63 ± 0.60
Total Nitrogen (g·kg^{-1})	0.20 ± 0.03
Alkali-hydrolyzable Nitrogen (mg·kg^{-1})	9.92 ± 0.58
Total Phosphorus (g·kg^{-1})	0.22 ± 0.01
Available Phosphorus (mg·kg^{-1})	2.81 ± 0.36
Total Potassium (g·kg^{-1})	7.01 ± 0.34
Available Potassium (mg·kg^{-1})	22.51 ± 0.27

Values are mean ± standard error (n = 3).

compound fertilizer ($N:P_2O_5:K_2O$ = 15:15:15) was used for nutrient treatment.

The soil was collected from the Arboretum of South China Agricultural University. Before the experiment, the soil was air-dried, milled, and passed through a 1-cm sieve to remove debris. Each plastic pot (15.5 cm bottom diameter, 19.2 cm height) was filled with 5 kg of the soil. The basic properties of the soil are shown in Table 1.

2.3 Experimental design

This study employed a two-factor factorial design, examining the effects of soil water content and fertilizer rate. Three distinct soil water levels were established at 55%, 75%, and 95% of field capacity, corresponding to deficit, optimal, and excessive water conditions (Griffiths and Parry, 2002; Brady and Weil, 2016). The four fertilizer levels (0, 6, 12, and 18 g pot^{-1} of $N:P_2O_5:K_2O$ = 15:15:15 compound fertilizer) were scaled from nursery application rates reported for containerized subtropical conifer seedlings (Fu et al., 2024) and adjusted for the 5 kg soil mass per pot and the background nutrient status of the experimental soil (Table 1), spanning no, low, medium, and high fertilization relative to conventional nursery practice for this container size. The combination of 75% field capacity and 0 g pot^{-1} served as the control (CK) (Quan et al., 2025), representing conventional nursery practice in South China, where container-grown seedlings of *C. tabularis* are typically maintained at approximately 75% field capacity without fertilizer. The fully crossed design resulted in 12 treatments (see Table 2), each with 5 replicates, totaling 60 pots. The experiment commenced on September 15, 2022, and continued for a duration of 10 months.

Fertilizer was applied 1 month after transplanting, once seedlings had established new leaf growth following transplant shock. To prevent root burn, we split the total fertilizer into two equal portions and added them in mid-October and mid-March. For application, we dug two holes on opposite sides of each seedling, 5 cm from the root collar and 5 cm deep. We placed equal fertilizer amounts into each hole. We started soil water content control after the first fertilization. We used the whole-pot weighing method, and checked readings with a portable soil moisture, temperature and salinity meter (FOM/mts). The control period ran from October 14 to July 2. We

TABLE 2 Experimental design.

Treatment	Soil water content (% of field capacity)	Compound fertilizer rate (g pot^{-1})
$W_{95}F_0$	95	0
$W_{95}F_6$	95	6
$W_{95}F_{12}$	95	12
$W_{95}F_{18}$	95	18
$W_{75}F_6$	75	6
$W_{75}F_{12}$	75	12
$W_{75}F_{18}$	75	18
$W_{55}F_0$	55	0
$W_{55}F_6$	55	6
$W_{55}F_{12}$	55	12
$W_{55}F_{18}$	55	18
CK	75	0

measured soil water daily and replenished water with 500-mL, 300-mL and 100-mL beakers (accuracy: 10 mL). To calculate the irrigation volume for each pot, we first found the water deficit by subtracting the current soil water content from the target field capacity. Then we divided that deficit by the bulk density, multiplied by the soil mass per pot, and finally divided by the density of water.

2.4 Determination and calculation of indicators

2.4.1 Indicator determination

Seedling height and ground diameter were measured monthly. Growth traits were analyzed at final harvest to avoid pseudoreplication across repeated measurements. At the final harvest, plants were separated into roots, stems, and leaves, and dried at 65 °C to a constant weight after initial heat inactivation at 105 °C for 30 min. Total biomass was calculated as the sum of all organ dry weights. Dried samples were digested using H_2SO_4-H_2O_2. Total N, P, and K contents were determined by Nessler's colorimetry, molybdenum-antimony spectrophotometry, and atomic absorption spectrophotometry, respectively.

The apparent fertilizer use efficiency (AFUE) for N, P, and K, instantaneous water use efficiency (WUEi), greenhouse gas (GHG) flux (F), and cumulative GHG emissions (E) were calculated using Equations (1)–(4), respectively:

$$\mathrm{AFUE} = \frac{U_F - U_0}{F_A} \times 100\% \tag{1}$$

where U_F is the above-ground nutrient (N, P, or K) accumulation in the fertilized treatment (g), U_0 is the above-ground nutrient accumulation in the unfertilized treatment under the corresponding water regime (g), and F_A is the total amount of the specific nutrient applied (g).

Leaf photosynthetic traits were measured using a Li-6400XT Portable Photosynthesis System (LI-COR Inc., Lincoln, NE, USA) between 9:00 and 11:30 a.m. on clear days in May 2023. Three fully expanded functional leaves per seedling (specifically the 4th to 6th leaves from the top) were selected for measurement. During the assessments, the CO_2 concentration, leaf temperature, and relative humidity were maintained at 400 ± 10 μmol·mol^{-1}, 25 °C ± 1 °C and 50%–70%, respectively. The photosynthetically active radiation (PAR) was set at 1,000 μmol·m^{-2}·s^{-1}. The measured parameters included the net photosynthetic rate (*P*n), transpiration rate (*T*r), stomatal conductance (*G*s), and intercellular CO_2 concentration (*C*i).

The instantaneous water use efficiency (WUEi) was calculated using the following equation:

$$\text{WUEi} = \frac{Pn}{Tr} \tag{2}$$

where *P*n is the net photosynthetic rate; *T*r is the transpiration rate.

Soil gas samples were collected using the static chamber method. Two cylindrical aluminum chambers (50 mm height, 90 mm diameter) were installed in each pot. Sampling was conducted between 9:00 a.m. and 12:00 p.m. in October and December 2022, and February, April, and June 2023. Gas was collected 0, 10, 20, and 30 min after chamber closure. Concentrations of CO_2, N_2O, and CH_4 were determined using an Agilent 7890A gas chromatograph (Agilent Technologies, USA). Soil greenhouse gas (GHG) fluxes $\left(F, mg \cdot m^{-2} \cdot h^{-1}\right)$ were calculated based on the linear change in gas concentration over the 30-min closure period using the following equation:

$$F = \rho \cdot \frac{V}{A} \cdot \frac{\Delta c}{\Delta t} \cdot \frac{273}{273 + T} \tag{3}$$

where ρ is the gas density at standard conditions, V is the chamber volume (m^3), A is the soil surface area (m^2), $Äc / Ät$ is the rate of concentration change over time, and T is the average air temperature (°C) inside the chamber during sampling.

Cumulative GHG emissions were derived by integrating the five sampling dates into one value per pot prior to ANOVA, so that each pot represented one independent unit. Total cumulative greenhouse gas emissions over these five periods were calculated using the following equation:

$$E = \sum_{i=1}^{5} \frac{\left(F_{i-1} + F_i\right) \times \left(d_i - d_{i-1}\right)}{2} \tag{4}$$

where E represents the total cumulative greenhouse gas emissions over five time periods (mg·m^{-2}), F_i denotes the greenhouse gas emissions in the current sampling period (mg·m^{-2}), F_{i-1} stands for the greenhouse gas emissions in the previous sampling period (mg·m^{-2}), d_i is the number of days in the current sampling period (d), and d_{i-1} refers to the number of days in the previous sampling period (d).

2.4.2 Comprehensive evaluation

Indicator selection followed a two-stage procedure: PCA was first used to reduce all candidate indicators to a set of principal components, and the indicator with the highest absolute loading on each retained component was selected as its representative for the subsequent EWM-TOPSIS evaluation. This PCA-based screening was performed to remove redundancy among highly intercorrelated variables prior to the comprehensive evaluation, rather than to select indicators after the fact.

Principal component analysis (PCA) was used to screen core indicators from the 19 original parameters (Greenacre et al., 2022). An integrated Entropy Weight Method (EWM) and TOPSIS model was applied to evaluate treatments and identify the optimal water-fertilizer regime (Li et al., 2019). EWM determined the objective weights, and TOPSIS ranked the comprehensive effects.

$$X = \left(x_{ij}\right) = \begin{bmatrix} x_{11} & x_{12} & \cdots & x_{1m} \\ x_{21} & x_{22} & \cdots & x_{2m} \\ \vdots & \vdots & \ddots & \vdots \\ x_{n1} & x_{n2} & \cdots & x_{nm} \end{bmatrix} \tag{5}$$

$$x'_{ij} = \frac{x_{ij} - \overline{x}_j}{s_j} \tag{6}$$

$$R = \frac{1}{n-1} X'^T X' \tag{7}$$

$$\eta_k = \frac{\lambda_k}{\sum_{k=1}^{m} \lambda_k} \tag{8}$$

$$\eta_k = \frac{\sum_{t=1}^{k} \lambda_t}{\sum_{t=1}^{m} \lambda_t} \tag{9}$$

To screen core evaluation indicators from the 19 original parameters across the 12 treatments, Principal Component Analysis (PCA) was employed. First, a raw evaluation matrix X was constructed (Equation 5). To eliminate dimensional effects and variance discrepancies among the original parameters, the data were standardized to obtain matrix X′ using Z-score standardization (Equation 6). The suitability of X' for PCA was confirmed by the Kaiser-Meyer-Olkin test (>0.6) and Bartlett's test of sphericity ($p < 0.05$). Subsequently, the correlation matrix R was calculated (Equation 7). The variance contribution rate (Equation 8) and cumulative variance contribution rate (Equation 9) were computed, retaining principal components with an initial eigenvalue greater than 1, which cumulatively accounted for 78.34% of the total variance. A standardized three-step method was employed to identify core indicators from the principal components for EWM-TOPSIS analysis. First, the indicator with the strongest loading in each component was retained. Second, if multiple indicators within the same component exhibited high loadings, only the strongest was kept to avoid redundancy. Third, we checked that the chosen indicators covered plant growth, nutrient accumulation, and environmental effects.

Based on strong loadings, comprehensive coverage, and independence, five indicators were ultimately selected: stem dry weight, root N content, stem P content, root K content, and cumulative CH_4 emissions.

$$Y=\left(y_{ij}\right)=\begin{bmatrix} y_{11} & y_{12} & \cdots & y_{1p} \\ y_{21} & y_{22} & \cdots & y_{2p} \\ \vdots & \vdots & \ddots & \vdots \\ y_{n1} & y_{n2} & \cdots & y_{np} \end{bmatrix} \quad (10)$$

$$y_{ij}'' = \frac{y_{ij}-\min\left(y_{1j},y_{2j},\ldots,y_{nj}\right)}{\max\left(y_{1j},y_{2j},\ldots,y_{nj}\right)-\min\left(y_{1j},y_{2j},\ldots,y_{nj}\right)} \quad (11)$$

$$y_{ij}'' = \frac{\max\left(y_{1j},y_{2j},\ldots,y_{nj}\right)-y_{ij}}{\max\left(y_{1j},y_{2j},\ldots,y_{nj}\right)-\min\left(y_{1j},y_{2j},\ldots,y_{nj}\right)} \quad (12)$$

$$y_{ij}' = y_{ij}'' + \varepsilon \quad (13)$$

$$p_{ij} = \frac{y_{ij}'}{\sum_{i=1}^{n} y_{ij}'} \quad (14)$$

$$e_j = -\frac{1}{\ln n}\sum_{i=1}^{n} p_{ij}\cdot \ln p_{ij} \quad (15)$$

$$g_j = 1-e_j \quad (16)$$

$$w_j = \frac{g_j}{\sum_{j=1}^{p} g_j} \quad (17)$$

$$Z=\left(z_{ij}\right)=\begin{bmatrix} y_{11}'w_1 & y_{12}'w_2 & \cdots & y_{1p}'w_p \\ y_{21}'w_1 & y_{22}'w_2 & \cdots & y_{2p}'w_p \\ \vdots & \vdots & \ddots & \vdots \\ y_{n1}'w_1 & y_{n2}'w_2 & \cdots & y_{np}'w_p \end{bmatrix} \quad (18)$$

$$A^{+} = \left(z_1^{+}, z_2^{+}, \ldots, z_p^{+}\right) \quad (19)$$

$$A^{-} = \left(z_1^{-}, z_2^{-}, \ldots, z_p^{-}\right) \quad (20)$$

$$D_i^{+} = \sqrt{\sum_{j=1}^{p}\left(z_{ij}-z_j^{+}\right)^2} \quad (21)$$

$$D_i^{-} = \sqrt{\sum_{j=1}^{p}\left(z_{ij}-z_j^{-}\right)^2} \quad (22)$$

$$C_i = \frac{D_i^{-}}{D_i^{+}+D_i^{-}} \quad (23)$$

An original evaluation matrix Y for these five indicators was constructed (Equation 10). The data were standardized for positive (Equation 11) and negative (Equation 12) indicators, followed by a non-negative translation to yield matrix Y' (Equation 13). Using the Entropy Weight Method (EWM), the value proportion p_{ij} (Equation 14), information entropy e_j (Equation 15), and objective weights w_j (Equations 16, 17) were determined. Finally, a weighted decision matrix Z was established (Equation 18) to identify the positive (A^+) and negative (A^-) ideal solutions (Equations 19, 20). Euclidean distances (D_i^+, D_i^-) were calculated (Equations 21, 22) to derive the relative closeness degree (C_i), which was used to rank the treatments (Equation 23).

2.5 Data analysis

A one-way ANOVA was conducted on all 12 treatment combinations to evaluate overall differences among the treatments, with mean separations conducted using Duncan's multiple range test ($p < 0.05$). In addition, a two-way ANOVA was utilized to partition the variance attributable to soil water content (W), fertilizer rate (F), and their interaction (W × F). All statistical analyses and comprehensive evaluations, including PCA-EWM-TOPSIS were carried out using SPSS 26.0 (IBM Corp., Armonk, NY, USA) and Microsoft Excel. Figures were generated using Origin 2021 (OriginLab Corp., Northampton, MA, USA).

3 Results

3.1 Plant growth traits

Water and fertilizer treatments, along with their interactions, significantly affected seedling growth and biomass (Figure 2). Compared to CK, the treatment $W_{55}F_{12}$ resulted in a 224% increase in total biomass and a 32% increase in root dry weight. A direct comparison between $W_{55}F_{12}$ and the unfertilized $W_{55}F_0$ indicated that fertilization alone led to a 315% increase in total biomass. At the 12 g fertilization rate, W_{55} produced 35% more biomass than W_{75}. Conversely, excessive water and fertilizer ($W_{95}F_{18}$) showed a strong inhibitory effect, reducing biomass and height increment by 54% and 62%, respectively, compared to CK. Within the W_{75} regime, F_{12} and F_{18} increased total biomass by 141 and 50% relative to F_0, respectively, whereas under W_{95}, F_{12} reduced biomass by 13% relative to F_0. The heatmap clearly illustrates that maintaining 95% field capacity severely restricts seedling growth regardless of fertilization (Figure 3). In contrast, combining 55% field capacity with a moderate fertilizer rate (12 g pot^{-1}) optimizes overall growth performance.

3.2 Nutrient uptake

Nutrient accumulation in each organ followed the order of leaf > stem > root across all treatments (Figure 4). For nitrogen and potassium, accumulation peaked at F_{12} and was highest under W_{55}. The $W_{55}F_{12}$ treatment yielded the maximum nitrogen and potassium accumulation, with increases of 701% and 318%, respectively, compared to CK. Phosphorus accumulation peaked at F_{12} under W_{75}, but at F_{18} under W_{55}. The highest phosphorus accumulation occurred in the $W_{55}F_{18}$ treatment, representing a

10.3389/ffgc.2026.1914270

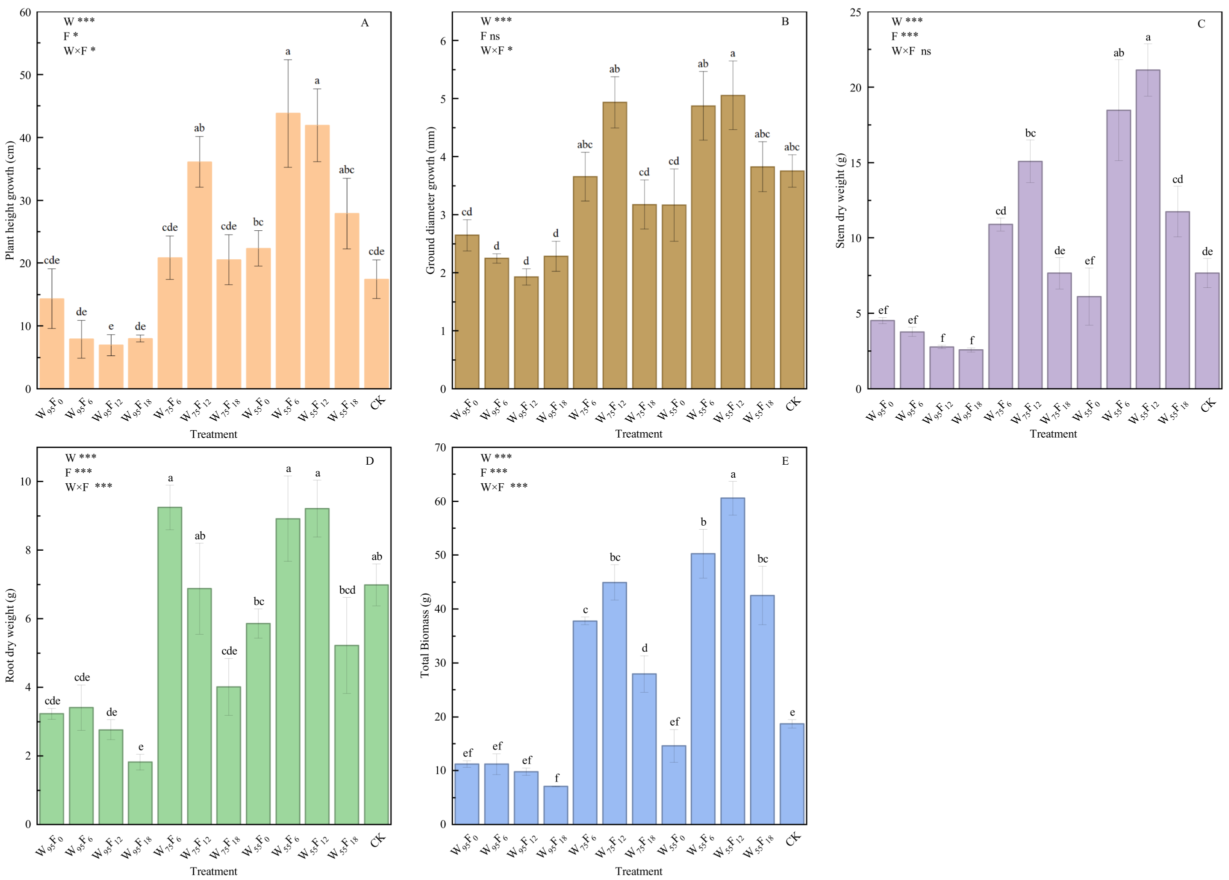

FIGURE 2
Effects of different water and fertilizer treatments on the growth of *C. tabularis* seedlings. **(A)** Plant height increment; **(B)** Ground diameter increment; **(C)** Stem dry weight; **(D)** Root dry weight; **(E)** Total biomass. W_{95}, W_{75}, and W_{55} denote 95%, 75%, and 55% of field capacity, respectively; F0, F6, F12, and F18 denote fertilizer rates of 0, 6, 12, and 18 g pot^{-1}; CK denotes the control treatment (75% field capacity, 0 g fertilizer). The different lowercase letters above the bars indicate significant differences among treatments at $p < 0.05$ according to Duncan's multiple range test. The results of the two-way ANOVA for the main effects of soil water content (W) and fertilizer rate (F), and their interaction (W × F) are shown in the upper left corner of each panel. ns means differences are not significant ($p > 0.05$). *means differences are significant at the 0.05 level ($p < 0.05$). ** means differences are significant at the 0.01 level ($p < 0.01$). *** means differences are significant at the 0.001 level ($p < 0.001$). Error bars represent standard error.

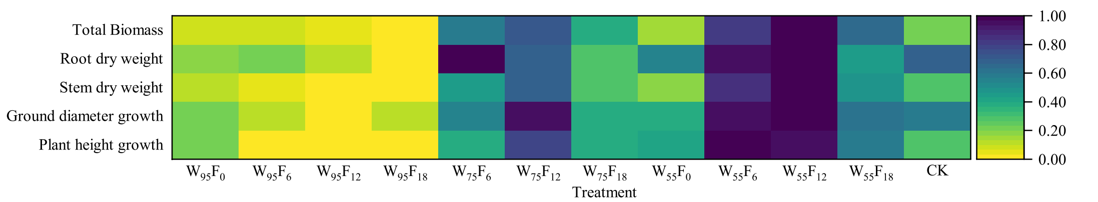

FIGURE 3
Heatmap of growth traits of *C. tabularis* seedlings. W_{95}, W_{75}, and W_{55} denote 95%, 75%, and 55% of field capacity, respectively; F0, F6, F12, and F18 denote fertilizer rates of 0, 6, 12, and 18 g pot^{-1}; CK denotes the control treatment (75% field capacity, 0 g fertilizer). The color bar on the right represents the normalized values of the growth indicators, ranging from 0.00 to 1.00. Yellow (values approaching 0.00) indicates lower relative growth values, while dark purple (values approaching 1.00) represents higher relative growth values. Data were normalized across all treatments to facilitate visual comparison of growth performance.

266% increase over the CK, followed by the $W_{55}F_{12}$ treatment with a 253% increase. Excessive irrigation (W_{95}) resulted in the lowest nutrient accumulation across all treatments. $W_{55}F_{12}$ increased root nitrogen, stem phosphorus, and root potassium accumulation by 173, 342, and 66%, respectively, relative to $W_{55}F_0$. Supplementary Table S2 presents the nutrient accumulation in roots, stems, and leaves across all 12 treatments (mean ± SE, $n = 3$).

The apparent fertilizer use efficiencies for N, P and K (AFUE-N, AFUE-P, and AFUE-K) were found to be optimal at $W_{55}F_6$ (Figure 5). Notably, AFUE-N at $W_{55}F_6$ was 22 and 931% higher than at $W_{75}F_6$ and $W_{95}F_6$, respectively, underscoring the significant influence of water regime on resource efficiency. In contrast, negative values for AFUE-P and AFUE-K were recorded under the W_{95} regimes, suggesting that the fertilized seedlings actually accumulated fewer nutrients than the CK under the same soil water content.

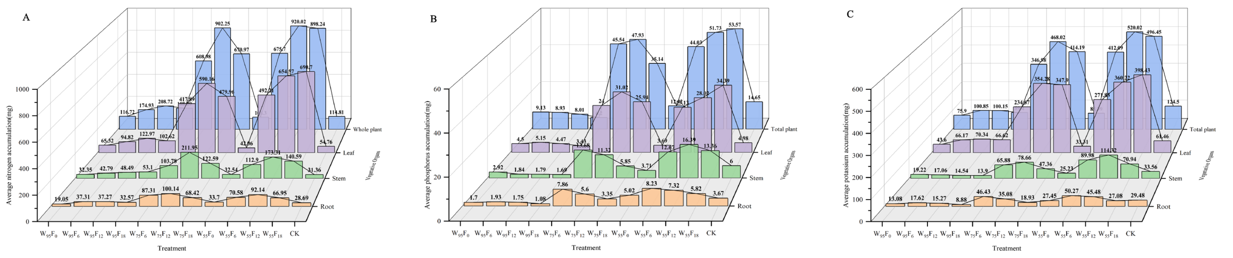

FIGURE 4
Effects of different water and fertilizer treatments on nutrient absorption of *C. tabularis* seedlings. **(A)** Nitrogen accumulation; **(B)** Phosphorus accumulation; **(C)** Potassium accumulation. W_{95}, W_{75}, and W_{55} denote 95%, 75%, and 55% of field capacity, respectively; F0, F6, F12, and F18 denote fertilizer rates of 0, 6, 12, and 18 g pot^{-1}; CK denotes the control treatment (75% field capacity, 0 g fertilizer). The 3D bar charts illustrate the distribution of nutrient accumulation across different vegetative organs (root, stem, and leaf) as well as the total plant under the 12 treatment combinations. The numbers above the bars represent the specific mean values of nutrient accumulation (mg) for each organ and treatment.

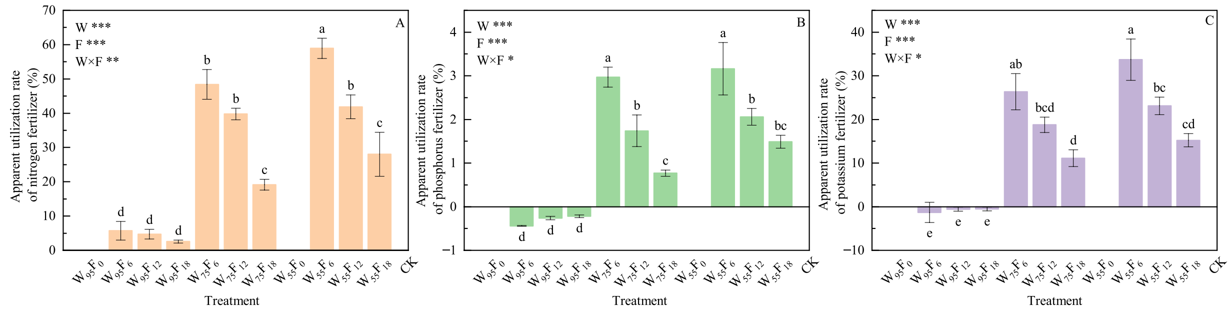

FIGURE 5
Effects of different water and fertilizer treatments on the apparent fertilizer use efficiency of *C. tabularis* seedlings. **(A)** Apparent fertilizer use efficiency of nitrogen fertilizer; **(B)** Apparent fertilizer use efficiency of phosphorus fertilizer; **(C)** Apparent fertilizer use efficiency of potassium fertilizer. W_{95}, W_{75}, and W_{55} denote 95%, 75%, and 55% of field capacity, respectively; F0, F6, F12, and F18 denote fertilizer rates of 0, 6, 12, and 18 g pot^{-1}; CK denotes the control treatment (75% field capacity, 0 g fertilizer). Bars for treatments without fertilizer application (F_0 treatments and CK) are absent because apparent fertilizer use efficiency is not applicable when no fertilizer is applied. The different lowercase letters above the bars indicate significant differences among treatments at $p < 0.05$ according to Duncan's multiple range test. The results of the two-way ANOVA for the main effects of soil water content (W) and fertilizer rate (F), and their interaction (W × F) are shown in the upper left corner of each panel. ns means differences are not significant ($p > 0.05$). *means differences are significant at the 0.05 level ($p < 0.05$). ** means differences are significant at the 0.01 level ($p < 0.01$). *** means differences are significant at the 0.001 level ($p < 0.001$). Error bars represent standard error.

3.3 Photosynthesis characteristics

*P*n peaked at $W_{75}F_6$, exhibiting a 33% increase compared to CK, but subsequently declined by 59% to 73% under the W_{95} treatment (Figure 6). *G*s reached its highest value at $W_{55}F_0$, being 77% higher than the CK, and was lowest in the $W_{75}F_{12}$ treatment, showing an 80% decrease compared to the CK. *C*i was significantly influenced by the interaction between water and fertilizer; under W_{75}, it increased by 115% at F_{12} and decreased by 65% at F_6 relative to the CK. *T*r was highest at F_0 for both W_{75} and W_{55}, while it was 83% lower than the CK at $W_{95}F_{18}$. Instantaneous water use efficiency reached its maximum at $W_{75}F_{12}$, demonstrating a 292% increase over the CK.

3.4 Cumulative soil greenhouse gas emissions

Under W_{95}, CO_2 emissions decreased with increased fertilization, peaking at F_{12} under both W_{55} and W_{75}. N_2O emissions showed distinct patterns across water regimes: under W_{95}, emissions rose progressively with fertilization rate; under W_{75}, emissions peaked at F_0; and under W_{55}, emissions reached their maximum at F_{12} (Figure 7). In terms of CH_4, net uptake was observed in $W_{95}F_{12}$, $W_{55}F_0$, $W_{55}F_{12}$, and $W_{55}F_{18}$, while net emissions were recorded in all other treatments.

3.5 Comprehensive evaluation

Based on the PCA results (Supplementary Table S1), five core indicators were identified: stem dry weight, root nitrogen content, stem phosphorus content, root potassium content, and cumulative CH_4 emissions. Among these indicators, stem dry weight had the highest weight (0.372), followed by root nitrogen content (0.232) and cumulative CH_4 emissions (0.155) (Table 3). According to the TOPSIS model (Table 4), $W_{55}F_{12}$ achieved the highest ranking, indicating the optimal combination of 55% field capacity and a 12 g fertilization rate. $W_{75}F_{12}$ and $W_{55}F_6$ also showed favorable performance due to effective water and fertilizer synergies. In contrast, $W_{95}F_0$ exhibited the poorest overall performance.

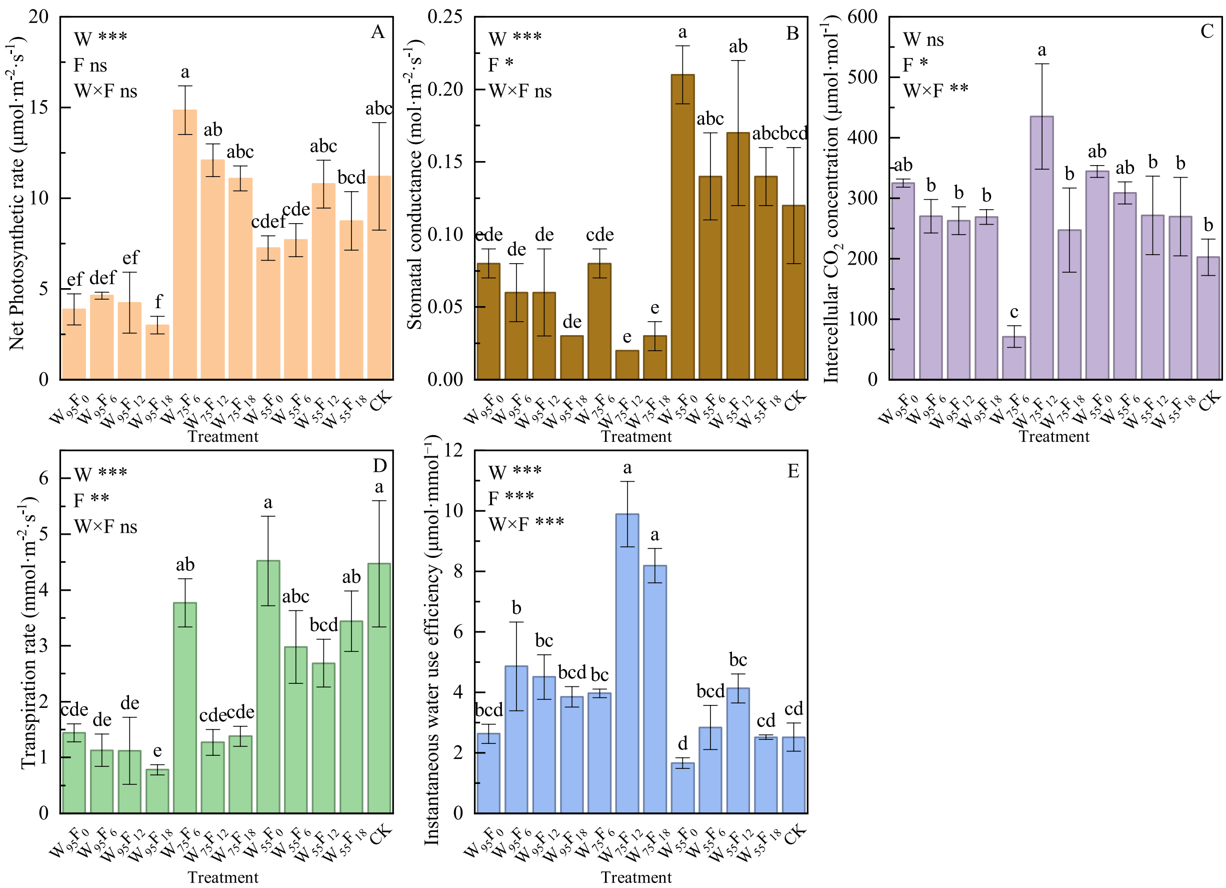

FIGURE 6
Effects of different water and fertilizer treatments on photosynthesis of *C. tabularis*. **(A)** Net photosynthetic rate; **(B)** Stomatal conductance; **(C)** Intercellular CO_2 concentration; **(D)** Transpiration rate. **(E)** Instantaneous water use efficiency. W_{95}, W_{75}, and W_{55} denote 95%, 75%, and 55% of field capacity, respectively; F0, F6, F12, and F18 denote fertilizer rates of 0, 6, 12, and 18 g pot^{-1}; CK denotes the control treatment (75% field capacity, 0 g fertilizer). The different lowercase letters above the bars indicate significant differences among treatments at $p < 0.05$ according to Duncan's multiple range test. The results of the two-way ANOVA for the main effects of soil water content (W) and fertilizer rate (F), and their interaction (W × F) are shown in the upper left corner of each panel. ns means differences are not significant ($p > 0.05$). *means differences are significant at the 0.05 level ($p < 0.05$). ** means differences are significant at the 0.01 level ($p < 0.01$). *** means differences are significant at the 0.001 level ($p < 0.001$). Error bars represent standard error.

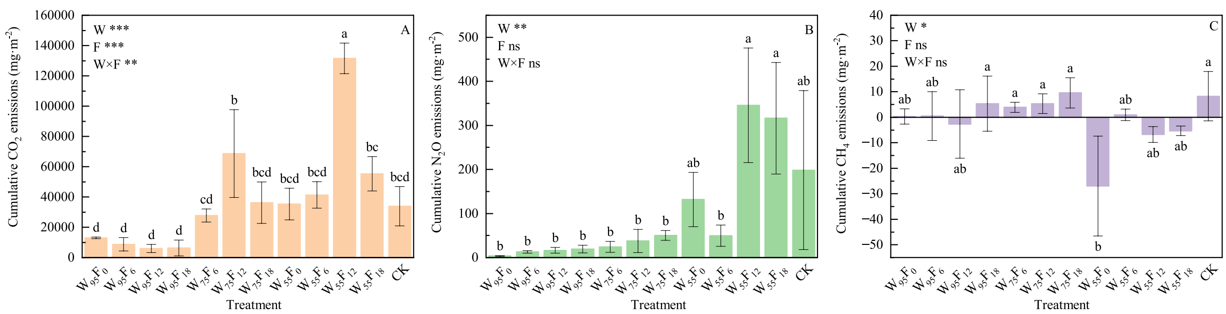

FIGURE 7
Effects of different water and fertilizer treatments on cumulative emissions of soil greenhouse gases. **(A)** Cumulative CO_2 emissions; **(B)** Cumulative N_2O emissions; **(C)** Cumulative CH_4 emissions. W_{95}, W_{75}, and W_{55} denote 95%, 75%, and 55% of field capacity, respectively; F0, F6, F12, and F18 denote fertilizer rates of 0, 6, 12, and 18 g pot^{-1}; CK denotes the control treatment (75% field capacity, 0 g fertilizer). The different lowercase letters above the bars indicate significant differences among treatments at $p < 0.05$ according to Duncan's multiple range test. The results of the two-way ANOVA for the main effects of soil water content (W) and fertilizer rate (F), and their interaction (W × F) are shown in the upper left corner of each panel. Ns means differences are not significant ($p > 0.05$). * means differences are significant at the 0.05 level ($p < 0.05$). ** means differences are significant at the 0.01 level ($p < 0.01$). *** means differences are significant at the 0.001 level ($p < 0.001$). Error bars represent standard error.

TABLE 3 Entropy weight results of comprehensive evaluation indices for water and fertilizer coupling of *C. tabularis* seedlings.

Indicator	Weight
Stem dry weight	0.372
Root Nitrogen content	0.232
Stem Phosphorus content	0.134
Root Potassium content	0.107
Cumulative CH_4 emissions	0.155

TABLE 4 TOPSIS entropy-weighted evaluation of water and fertilizer coupling effects on *C. tabularis* seedling performance.

Treatment	Relative closeness coefficient	Rank
$W_{95}F_0$	0.165	12
$W_{95}F_6$	0.231	10
$W_{95}F_{12}$	0.294	8
$W_{95}F_{18}$	0.347	7
$W_{75}F_6$	0.428	5
$W_{75}F_{12}$	0.572	2
$W_{75}F_{18}$	0.415	6
$W_{55}F_0$	0.263	9
$W_{55}F_6$	0.549	3
$W_{55}F_{12}$	0.638	1
$W_{55}F_{18}$	0.495	4
CK	0.224	11

W_{95}, W_{75}, and W_{55} denote 95%, 75%, and 55% of field capacity, respectively; F0, F6, F12, and F18 denote fertilizer rates of 0, 6, 12, and 18 g pot^{-1}; CK denotes the control treatment (75% field capacity, 0 g fertilizer).

4 Discussion

4.1 Growth and nutrient uptake

Water stress is widely recognized as a primary growth-limiting factor in plantation seedlings (Xu et al., 2022); however, its effects vary considerably with irrigation intensity. The W_{95} treatment suppressed plant height, ground diameter, and total biomass, likely due to excessive irrigation, which reduced aeration porosity and induced root hypoxia. Under such anaerobic conditions, the uptake pathways for phosphorus and potassium are disrupted (Wang et al., 2011; Hou et al., 2021), consistent with the decline in phosphorus and potassium accumulation we observed under W_{95} across all fertilization levels. Notably, high fertilization inputs failed to reverse this suppression, suggesting that nutrient supplementation cannot compensate for oxygen-limited root function. We note, however, that root oxygen status was not directly measured; the hypothesized role of root hypoxia under W_{95} should therefore be confirmed by future dissolved-O_2 or aerenchyma assessments.

Conversely, *C. tabularis* exhibited strong adaptability to W_{55}. When combined with F_{12}, W_{55} increased total biomass by 224% over the CK, a value comparable to the 180%–240% increases typically reported for highly adaptable broadleaved species (Zhang et al., 2020; Zhou et al., 2022). While 75% field capacity is widely considered optimal for many agronomic crops, it exceeds the physiological aeration threshold for *C. tabularis* seedlings in a containerized environment. As a high-value timber species primarily distributed in well-drained upland forests across tropical and subtropical Asia, *C. tabularis* is evolutionarily adapted to high soil aeration and may possess innate sensitivity to even moderate reductions in soil oxygen availability. This study's findings indicate that the superior performance under 55% field capacity (W_{55}) compared to 75% (W_{75}) likely reflects the species' specific eco-physiological requirement for a well-aerated rhizosphere, which W_{55} provided through a more favorable air-to-water ratio. The significant increase in biomass at $W_{55}F_{12}$ suggests that this soil water content aligns better with the fast-draining soil conditions of its natural habitat, thereby facilitating more efficient root respiration, nutrient uptake, and radial transport compared to the relatively wetter W_{75} treatment.

4.2 Photosynthetic physiology and greenhouse gas emissions

Leaf photosynthesis and soil GHG emissions jointly determine the net carbon balance of plantation ecosystems (Jiang et al., 2020; Yu et al., 2022). Water availability significantly influenced the *Pn*, *Gs*, and *Tr* of *C. tabularis*; however, the direction of these effects was strongly dependent on the fertilization rate. Under W_{75}, low fertilization (F_6) maximized *Pn*, while medium to high fertilization (F_{12}, F_{18}) reduced *Gs* and *Tr* without a proportional reduction in *Pn*, indicating a shift towards stomatal water conservation rather than maximization of carbon gain. This pattern of stomatal adjustment reduced stomatal conductance while maintaining stable assimilation rates, consistent with stomatal regulation patterns that balance carbon gain and water loss under adequate water supply, as documented in other plantation species (Jhou et al., 2017). Furthermore, this suggests that *C. tabularis* can enhance instantaneous water use efficiency through fertilization under sufficient water availability. Under W_{55} conditions, $W_{55}F_{12}$ seedlings achieved the highest total biomass despite a moderate single-leaf *Pn*, driven by a substantially larger total leaf biomass that maximized whole-plant carbon assimilation. Interestingly, the highest *Gs* was observed in the unfertilized $W_{55}F_0$. This is likely due to the seedlings' small size and low transpirational demand, which slowed soil water depletion and allowed stomata to remain open. In contrast, the larger canopies of $W_{55}F_{12}$ depleted soil water content more rapidly. Coupled with fertilizer-induced osmotic stress, this likely triggered stronger root-to-shoot ABA signaling (Tardieu and Simonneau, 1998) for stomatal down-regulation to ensure hydraulic safety. Nevertheless, the robust nutrient uptake in $W_{55}F_{12}$ effectively maintained steady photosynthetic carbon gains, maximizing overall growth. Because neither xylem ABA concentration nor leaf osmotic potential was measured, the proposed ABA-mediated stomatal regulation and osmotic stress remain hypotheses requiring direct physiological confirmation.

Because gas sampling was conducted on five occasions over the 10-month experiment, the cumulative flux estimates presented below should be interpreted as coarse, seasonally resolved approximations rather than precise annual budgets; the following comparisons among treatments are therefore discussed as directional patterns rather than precisely quantified differences. Within this constraint, soil GHG dynamics exhibited a pattern distinct from the photosynthetic responses, yet both were sensitive to the water-fertilizer interaction. Cumulative CO_2 emissions were highest under W_{55} and W_{75}, peaking at $W_{55}F_{12}$, and significantly lower under W_{95}. We hypothesize that the suppressed CO_2 efflux under W_{95} reflects waterlogging-induced inhibition of aerobic decomposition, whereas the peak under $W_{55}F_{12}$ may reflect a combination of adequate soil aeration, enhanced root exudation, and elevated microbial activity (Chi et al., 2020); these mechanisms were not directly measured and require confirmation through soil microbial community or enzyme activity assays. Notably, the well-aerated W_{55} condition coincided with a shift in soil CH_4 dynamics from net emission to net uptake. Waterlogged conditions (W_{95}) generally promoted CH_4 emission, consistent with enhanced methanogenesis and suppressed methanotrophy under anaerobic conditions, but CH_4 uptake was also observed at $W_{95}F_{12}$; we hypothesize that moderate nutrient input may partially support methane-oxidizing activity even under oxygen-limited conditions (Feng et al., 2020), though this remains speculative in the absence of direct measurement of methanotroph abundance or activity.

The comparatively high soil CO_2 efflux under $W_{55}F_{12}$ occurred alongside the highest photosynthetic rate and total biomass observed among all treatments, indicating strong carbon assimilation capacity at this treatment. However, because our measurements were limited to leaf-level *P*n and soil GHG fluxes rather than a complete net ecosystem carbon budget, and because CO_2, CH_4, and N_2O were not converted to a common CO_2-equivalent basis, we cannot quantify whether photosynthetic carbon gains under $W_{55}F_{12}$ offset soil respiratory and other GHG losses, and we do not interpret these results as evidence of an improved net carbon balance. A full assessment of the net warming potential associated with each water-fertilizer combination would require CO_2-equivalent accounting across all three gases together with higher-frequency flux sampling, which we identify as a priority for future work.

4.3 Resource use efficiency

The negative AFUE values under W_{95} indicate that excessive irrigation completely negated the benefits of fertilization. This phenomenon likely occurred due to high soil water content, which caused root hypoxia and severely limited active nutrient uptake. Furthermore, the excess irrigation water led to the loss of unabsorbed fertilizers through leaching. The fertilization rate significantly influenced resource use efficiency with a clear ceiling effect observed. Although adequate nutrients improve root hydraulic conductivity and water uptake (Bauer et al., 2025), F_{18} consistently reduced AFUE across all water regimes. This limitation aligns with the potential suppression of nutrient absorption caused by osmotic stress resulting from excessive fertilizer concentrations (Zheng et al., 2011). F_6 maximized fertilizer efficiency while F_{12} improved seedling quality without significantly compromising AFUE. This suggests that the cultivation objective, rather than adhering to a single fixed optimum rate, should guide fertilization decisions: F_6 for fertilizer-efficiency-oriented nurseries, and F_{12} for scenarios where seedling quality is the primary target. These mechanistic interpretations, root hypoxia, nutrient leaching, and osmotic stress, were not directly measured and should be regarded as hypotheses to be tested in future targeted experiments.

4.4 Optimal irrigation and fertilizer management

Optimizing irrigation and fertilization necessitates a balance between growth, resource efficiency, and ecological impact. In this study, $W_{55}F_{12}$ yielded the highest biomass and seedling quality, albeit with relatively high greenhouse gas emissions. Conversely, $W_{95}F_{18}$ involved maximum fertilizer input but exhibited inhibited growth and reduced efficiency, highlighting evident trade-offs in practical production. Although $W_{75}F_6$ maximized single-leaf net photosynthetic rate, this leaf-level measurement was not among the five core indicators retained for the comprehensive evaluation, because it loaded on the same principal component as, but less strongly than, stem dry weight. The comparatively low overall ranking of $W_{75}F_6$ (C_i = 0.428, rank 5) relative to $W_{55}F_{12}$ (C_i = 0.638, rank 1) therefore reflects the fact that superior instantaneous photosynthesis at the leaf scale did not translate into superior whole-plant biomass accumulation, nutrient uptake, or cumulative CH_4 performance. A comprehensive evaluation using the PCA-EWM-TOPSIS model revealed that $W_{55}F_{12}$ had the highest relative closeness degree, providing a scientific basis for *C. tabularis* seedling cultivation in the subtropical region.

However, the approximately two-month sampling intervals and confined pots may introduce uncertainties in cumulative GHG estimation and root development. Greenhouse temperature occasionally fell as low as 5.5 °C on the coldest nights, well below the 22.8 °C mean; brief cold excursions cannot be ruled out as a contributing factor to the reduced fluxes and slower growth observed in the December sampling campaign. Given that this study was conducted in pot experiments, future field trials are recommended. Additionally, long-term, high-frequency monitoring throughout growth stages is essential to develop a comprehensive water and fertilizer regulation strategy for *C. tabularis*.

5 Conclusion

This one-year pot experiment highlights the importance of coordinated water and fertilizer management for improving the growth performance and environmental sustainability of *C. tabularis* seedlings. Soil water serves as the primary driver of the biomass accumulation and height growth of *C. tabularis*, while the interactions between water and fertilizer regulated root development and biomass allocation. A field capacity of 55% optimizes fertilizer efficiency; however, excessive irrigation or over-fertilization can severely inhibit growth. This well-aerated condition combined with optimal fertilization mitigated greenhouse gas emissions, shifting soil CH_4 from net emission to net uptake. Comprehensive evaluation using PCA-EWM-TOPSIS confirmed that a field capacity of 55% with 12 g pot^{-1} compound fertilizer achieves an ideal balance among growth, resource use efficiency, and ecological trade-offs. These findings are based on a one-year pot experiment under greenhouse conditions; field trials across different soil types, climates, and stand ages are required before recommending $W_{55}F_{12}$ for operational nursery or plantation management.

Data availability statement

The original contributions presented in the study are included in the article/Supplementary material, further inquiries can be directed to the corresponding authors.

Author contributions

HQ: Conceptualization, Data curation, Formal analysis, Methodology, Software, Validation, Visualization, Writing – original draft, Writing – review & editing. JL: Data curation, Formal analysis, Investigation, Methodology, Supervision, Validation, Writing – review & editing. SZ: Conceptualization, Funding acquisition, Project administration, Resources, Supervision, Writing – review & editing. SC: Conceptualization, Data curation, Methodology, Supervision, Validation, Writing – review & editing.

Funding

The author(s) declared that financial support was received for this work and/or its publication. This research was funded by the Forestry Science and Technology Innovation Project of Guangdong Province (2022KJCX015).

Conflict of interest

The author(s) declared that this work was conducted in the absence of any commercial or financial relationships that could be construed as a potential conflict of interest.

Generative AI statement

The author(s) declared that Generative AI was not used in the creation of this manuscript.

Any alternative text (alt text) provided alongside figures in this article has been generated by Frontiers with the support of artificial intelligence and reasonable efforts have been made to ensure accuracy, including review by the authors wherever possible. If you identify any issues, please contact us.

Publisher's note

Supplementary material

The Supplementary material for this article can be found online at: https://www.frontiersin.org/articles/10.3389/ffgc.2026.1914270/full#supplementary-material

References

Alderotti, F., Lo Piccolo, E., Brunetti, C., Stefano, G., Ugolini, T., Cecchi, L., et al. (2025). Cultivar-specific responses of young olive trees to water deficit: impacts on physiology, leaf anatomy, and fruit quality in 'arbequina', 'leccio del corno' and 'maurino'. *Plant Physiol. Biochem.* 229:110331. doi: 10.1016/j.plaphy.2025.110331

An, Y., Li, Q., and Zhang, L. (2022). Managing agricultural water use in a changing climate in China. *Sustain. Prod. Consump.* 33, 978–990. doi: 10.1016/j.spc.2022.08.023

Bauer, F. M., Baker, D. N., Giraud, M., Baca Cabrera, J. C., Vanderborght, J., Lobet, G., et al. (2025). Root system architecture reorganization under decreasing soil phosphorus lowers root system conductance of *Zea mays*. *Ann. Bot.* 136, 973–986. doi: 10.1093/aob/mcae198

Binkley, D., and Fisher, R. F. (2019). "Nutrition management," in *Ecology and Management of Forest Soils*, (Hoboken: Wiley), 319–349.

Brady, N. C., and Weil, R. R. (2016). *The Nature and Properties of Soils*. 15th Edn Upper Saddle River: Pearson.

Campoe, O. C., Stape, J. L., Albaugh, T. J., Allen, H. L., Fox, T. R., Rubilar, R., et al. (2013). Fertilization and irrigation effects on tree level aboveground net primary production, light interception and light use efficiency in a loblolly pine plantation. *For. Ecol. Manag.* 288, 43–48. doi: 10.1016/j.foreco.2012.05.026

Chen, Y., Zhang, J., Chen, M., Zhu, F., and Song, T. (2023). Optimizing water conservation and utilization with a regulated deficit irrigation strategy in woody crops: a review. *Agric. Water Manag.* 289:108523. doi: 10.1016/j.agwat.2023.108523

Chi, Y., Yang, P., Ren, S., Ma, N., Yang, J., and Xu, Y. (2020). Effects of fertilizer types and water quality on carbon dioxide emissions from soil in wheat-maize rotations. *Sci. Total Environ.* 698:134010. doi: 10.1016/j.scitotenv.2019.134010

Feng, H., Guo, J., Han, M., Wang, W., Peng, C., Jin, J., et al. (2020). A review of the mechanisms and controlling factors of methane dynamics in forest ecosystems. *For. Ecol. Manag.* 455:117702. doi: 10.1016/j.foreco.2019.117702

Fu, Y., Ding, G., Quan, W., Zhao, X., and Tao, Q. (2024). Coupling optimization of water-fertilizer for coordinated development of the environment and growth of *Pinus massoniana* seedlings. *Agric. Water Manag.* 300:108895. doi: 10.1016/j.agwat.2024.108895

Greenacre, M., Groenen, P. J. F., Hastie, T., D'Enza, A. I., Markos, A., and Tuzhilina, E. (2022). Principal component analysis. *Nat. Rev. Methods Primers* 2:100. doi: 10.1038/s43586-022-00184-w

Griffiths, H., and Parry, M. A. J. (2002). Plant responses to water stress. *Ann. Bot.* 89, 801–802. doi: 10.1093/aob/mcf159

Hou, K., Huang, Y., Rong, X., Peng, J., Tian, C., and Han, Y. (2021). The effects of the depth of fertilization on losses of nitrogen and phosphorus and soil fertility in the red paddy soil of China. *PeerJ* 9:e11347. doi: 10.7717/peerj.11347

Hussain, F., Ahmed, S., Muhammad Zaigham Abbas Naqvi, S., Awais, M., Zhang, Y., Zhang, H., et al. (2025). Agricultural non-point source pollution: comprehensive analysis of sources and assessment methods. *Agriculture* 15:531. doi: 10.3390/agriculture15050531

Islam, M., Rahman, M., and Bräuning, A. (2018). Xylem anatomical responses of diffuse porous *Chukrasia tabularis* to climate in a south Asian moist tropical forest. *For. Ecol. Manag.* 412, 9–20. doi: 10.1016/j.foreco.2018.01.035

Jhou, H., Wang, Y., Wu, C., Yu, J., and Chen, C. (2017). Photosynthetic gas exchange responses of *Swietenia macrophylla* king and *Melia azedarach* l. plantations under drought conditions. *Bot. Stud.* 58:57. doi: 10.1186/s40529-017-0212-8

Jiang, M., Medlyn, B. E., Drake, J. E., Duursma, R. A., Anderson, I. C., Barton, C. V. M., et al. (2020). The fate of carbon in a mature forest under carbon dioxide enrichment. *Nature* 580, 227–231. doi: 10.1038/s41586-020-2128-9

Li, M., Sun, H., Singh, V. P., Zhou, Y., and Ma, M. (2019). Agricultural water resources management using maximum entropy and entropy-weight-based TOPSIS methods. *Entropy* 21:364. doi: 10.3390/e21040364

Luo, L., Li, R., Ma, D., Wang, Y., and Wang, L. (2024). Effects of water-fertilizer coupling on growth characteristics and water use efficiency of *Camellia petelotii* seedlings. *Phyton-Int. J. Exp. Bot.* 93, 2927–2947. doi: 10.32604/phyton.2024.056429

Quan, H. T., Zhu, J. Y., Long, F. L., Zhao, Q., Wu, D. M., and Zeng, S. C. (2025). Responses of growth and physiological characteristics of *Chukrasia tabularis* seedlings to drought stress (in Chinese). *J. South China Agric. Univ.* 46, 587–595. doi: 10.7671/j.issn.1001-411X.202412005

Rabbai, A., Barba, J., Canducci, M., Hart, K. M., Mackenzie, A. R., Kettridge, N., et al. (2024). Fertilization-induced greenhouse gas emissions partially offset carbon sequestration during afforestation. *Soil Biol. Biochem.* 199:109577. doi: 10.1016/j.soilbio.2024.109577

Tardieu, F., and Simonneau, T. (1998). Variability among species of stomatal control under fluctuating soil water status and evaporative demand: modelling isohydric and anisohydric behaviours. *J. Exp. Bot.* 49, 419–432. doi: 10.1093/jxb/49.Special_Issue.419

Tariq, A., Pan, K., Olatunji, O. A., Graciano, C., Li, Z., Sun, F., et al. (2017). Phosphorous application improves drought tolerance of *Phoebe zhennan*. *Front. Plant Sci.* 8:1561. doi: 10.3389/fpls.2017.01561

Wang, L., Liang, T., Chong, Z., and Zhang, C. (2011). Effects of soil type on leaching and runoff transport of rare earth elements and phosphorous in laboratory experiments. *Environ. Sci. Pollut. Res. Int.* 18, 38–45. doi: 10.1007/s11356-010-0357-4

Wilson, M. J., He, Z., and Yang, X. (2004). *The Red Soils of China: Their Nature, Management and Utilization*. Dordrecht: Springer.

Wright, S. J., Yavitt, J. B., Wurzburger, N., Turner, B. L., Tanner, E. V. J., Sayer, E. J., et al. (2011). Potassium, phosphorus, or nitrogen limit root allocation, tree growth, or litter production in a lowland tropical forest. *Ecology* 92, 1616–1625. doi: 10.1890/10-1558.1

Xu, X., Yue, Q., Wu, H., Guo, S., Zhang, C., and Guo, P. (2022). Coupling optimization of irrigation and fertilizer for synergic development of economy-resource-environment: a generalized inexact quadratic multi-objective programming. *J. Clean. Prod.* 361:132115. doi: 10.1016/j.jclepro.2022.132115

Yu, T., Lu, F., Yang, S., Zhang, L., Huang, B., Wang, X., et al. (2022). Greenhouse gas budget and net carbon sequestration of different afforestation types used in grain for green project —a case study in central south and East China. *Bull. Soil Water Conserv.* 42, 337–347. doi: 10.13961/j.cnki.stbctb.2022.05.041

Zhang, Z., Tariq, A., Zeng, F., Graciano, C., and Zhang, B. (2020). Nitrogen application mitigates drought-induced metabolic changes in *Alhagi sparsifolia* seedlings by regulating nutrient and biomass allocation patterns. *Plant Physiol. Biochem.* 155, 828–841. doi: 10.1016/j.plaphy.2020.08.036

Zheng, C., Ji, D., Liu, W., Qiu, J., Wu, J., Chen, S., et al. (2011). Eco-physiological responses of high-latitude transplanted *Aegiceras corniculatum* seedlings to NaCl stress. *Chin. J. Appl. Ecol.* 22, 2279–2284. doi: 10.13287/j.1001-9332.2011.02440

Zhou, H., Hou, L., Lv, X., Yang, G., Wang, Y., and Wang, X. (2022). Compensatory growth as a response to post-drought in grassland. *Front. Plant Sci.* 13:1004553. doi: 10.3389/fpls.2022.1004553